11-2014

100-ps-pulse-duration, 100-J burst-mode laser for kHz–MHz flow diagnostics

Sukesh Roy
Spectral Energies

Joseph D. Miller
Air Force Research Laboratory

Mikhail N. Slipchenko
Spectral Energies

Paul S. Hsu
Spectral Energies

Jason G. Mance
Spectral Energies

See next page for additional authors

100-ps-pulse-duration, 100-J burst-mode laser for kHz–MHz flow diagnostics

Abstract
A high-speed, master-oscillator power-amplifier burst-mode laser with ~100 ps pulse duration is demonstrated with output energy up to 110 J per burst at 1064 nm and second-harmonic conversion efficiency up to 67% in a KD*P crystal. The output energy is distributed across 100 to 10,000 sequential laser pulses, with 10 kHz to 1 MHz repetition rate, respectively, over 10 ms burst duration. The performance of the 100 ps burst-mode laser is evaluated and been found to compare favorably with that of a similar design that employs a conventional ~8 ns pulse duration. The nearly transform-limited spectral bandwidth of 0.15 cm^{-1} at 532 nm is ideal for a wide range of linear and nonlinear spectroscopic techniques, and the 100 picosecond pulse duration is optimal for fiber-coupled spectroscopic measurements in harsh reacting-flow environments.

Keywords
conversion efficiency, laser diagnostics, mathematical transformations, power amplifiers, ultrashort pulses, flow environment, nonlinear spectroscopic techniques, Pico-second pulse, repetition rate, second-harmonic, spectral bandwidth

Disciplines
Mechanical Engineering

Comments
This article is from *Optics Letters* 39 (2014): 6462, doi: 10.1364/OL.39.006462. Posted with permission.

Authors
Sukesh Roy, Joseph D. Miller, Mikhail N. Slipchenko, Paul S. Hsu, Jason G. Mance, Terrence R. Meyer, and James R. Gord

100-ps-pulse-duration, 100-J burst-mode laser for kHz–MHz flow diagnostics

Sukesh Roy,[1,*] Joseph D. Miller,[2] Mikhail N. Slipchenko,[1] Paul S. Hsu,[1] Jason G. Mance,[1] Terrence R. Meyer,[3] and James R. Gord[2]

[1]*Spectral Energies, LLC, Dayton, Ohio 45431, USA*

[2]*Air Force Research Laboratory, Aerospace Systems Directorate, Wright-Patterson AFB, Ohio 45433, USA*

[3]*Department of Mechanical Engineering, Iowa State University, Ames, Iowa 50011, USA*

**Corresponding author: roy.sukesh@gmail.com*

Received September 30, 2014; revised October 14, 2014; accepted October 16, 2014; posted October 17, 2014 (Doc. ID 213514); published November 10, 2014

A high-speed, master-oscillator power-amplifier burst-mode laser with ~100 ps pulse duration is demonstrated with output energy up to 110 J per burst at 1064 nm and second-harmonic conversion efficiency up to 67% in a KD*P crystal. The output energy is distributed across 100 to 10,000 sequential laser pulses, with 10 kHz to 1 MHz repetition rate, respectively, over 10 ms burst duration. The performance of the 100 ps burst-mode laser is evaluated and been found to compare favorably with that of a similar design that employs a conventional ~8 ns pulse duration. The nearly transform-limited spectral bandwidth of 0.15 cm^{-1} at 532 nm is ideal for a wide range of linear and nonlinear spectroscopic techniques, and the 100 picosecond pulse duration is optimal for fiber-coupled spectroscopic measurements in harsh reacting-flow environments.

OCIS codes: (120.1740) Combustion diagnostics; (140.7090) Ultrafast lasers; (140.3280) Laser amplifiers; (140.3538) Lasers, pulsed.

http://dx.doi.org/10.1364/OL.39.006462

Understanding transient, high-temperature physical and chemical processes in reacting and nonreacting high-speed flows is critical for the development of predictive models and for improving the performance of next-generation subsonic, hypersonic, and rocket propulsion devices [1]. Measurements of temperature, velocity, and chemical-species concentrations at high bandwidth (typically 10 kHz–1 MHz) are required for providing better insight into processes, such as supersonic injection, fuel–air mixing, ignition, flame holding, turbulence–flame interactions, nonequilibrium chemistry, thermo-acoustic instabilities, and shock/boundary-layer interactions. Thus far, high-bandwidth measurements of such processes have been investigated primarily with linear spectroscopic techniques based on nanosecond (ns) laser architectures as first demonstrated by Wu and Miles [2] and recently reviewed by Thurow *et al.* [3].

The availability of commercial, turn-key picosecond (ps) and femtosecond (fs) laser systems has aided the advancement of nonlinear optical spectroscopic techniques such as coherent anti-Stokes Raman scattering (CARS) [4,5], two-photon planar laser-induced fluorescence (TPLIF) [6], and Raman-excited laser-induced electronic fluorescence (RELIEF) [7]. Because of quadratic and higher order dependences on excitation-beam power density, laser sources with sub-ns pulse duration are usually required for nonlinear spectroscopic measurements with high signal-to-noise ratio, especially for acquiring spatially and temporally resolved one- or two-dimensional data. Furthermore, sub-ns pulses have also been shown to improve the peak power available for nonlinear spectroscopic approaches when fiber-based laser delivery is utilized [5]. Fiber coupling is potentially important for propulsion devices with limited optical access and for measurements in harsh operating conditions.

Thus far, high-energy 100 ps, 10–20 Hz laser systems with hundreds of mJ/pulse have been used for measuring temperature and real-time collisional lifetimes of various molecular species [4,6,8]. Measurements of temperature and various chemical species are also being accomplished utilizing fs laser systems operating with ~1–15 mJ at low kHz rates [4,9]. In spite of many successful demonstrations, fs- and ps-laser-based nonlinear spectroscopic approaches have very limited spatial extent for chemical-species imaging [8,9] and low data-acquisition rates for two-dimensional temperature imaging [8]. This inhibits spatiotemporally resolved imaging and prevents high-fidelity comparison of experimental and numerical data related to turbulent reacting or hypersonic flows.

The limited repetition rate or pulse energy of continuously pulsed ps and fs laser systems originates from limited average output power. To overcome the average-power limitation of continuously pulsed lasers, one can utilize burst-mode operation. Burst-mode lasers achieve high pulse energy in combination with high-repetition-rate operation by grouping a series of closely spaced pulses into short bursts, thus enabling high pulse peak power and high repetition rate with low average system power. Several master-oscillator power-amplifier (MOPA) architectures and various active laser media have been used for producing bursts of fs, ps, and ns pulses, including Yb-doped fiber amplifiers [10,11], Yb:YAG thin-disk multipass amplifiers [12], multipass amplifiers based on a cryogenically cooled Yb^{3+}:CaF_2 crystal [13], multi-stage Nd:YLF amplifiers [14], and Nd:YAG multi-stage amplifiers [2,3,15–22].

While fiber-based amplifiers are the most robust, they are limited in pulse energy by the fiber-damage threshold. Among free-space burst-mode systems, Yb:YAG thin-disk amplifiers have the highest reported peak power, producing 800-fs, 100-kHz pulse sequences with up to 5 mJ per pulse [12]. This pulse energy is not sufficient to interrogate larger two-dimensional probe areas based on various nonlinear spectroscopic approaches [9], especially if the

pulse energy is used to pump frequency-conversion devices such as broadband dye lasers and optical parametric amplifiers. Moreover, to perform two-dimensional temperature measurements at 10–100 kHz over a reasonable area requires significantly higher power fs or ps pulses [8].

Among ns burst-mode systems, Nd:YAG multi-stage burst-mode lasers are capable of producing long burst durations of 10–100 ms [15,16] with high pulse energies up to a few Joules [17]. Such laser systems have been successfully used for linear optical-diagnostic techniques such as planar laser-induced fluorescence (PLIF) [18–20], simultaneous particle-image velocimetry (PIV) and PLIF mixture-fraction imaging [21], and Rayleigh and Raman scattering [3,17,22]. The narrow linewidth (<1 GHz) of ns burst-mode lasers has been an important advantage in these measurements for efficient coupling with molecular transitions. However, as noted earlier, the limited peak intensity is not optimal for performing high-speed nonlinear spectroscopic measurements such as CARS or multi-photon PLIF. These nonlinear techniques require high-peak-power, wavelength-tunable laser pulses. Hence, it is of interest to extend the operation of high-energy burst-mode systems to the sub-ns regime.

With regard to fiber delivery, the use of ns pulses for nonlinear spectroscopic techniques is also problematic because of the low damage threshold of the fibers compared to the pulse energy required for nonlinear spectroscopy in the ns regime [5]. The availability of a high-energy, sub-ns burst-mode laser would allow sufficient energy for pumping frequency-conversion devices and be suitable for fiber-based delivery. For example, it was shown that 100 ps pulses are optimal for fiber coupling in the case of single-shot CARS thermometry [5]. Although the 100 ps pulse duration is optimal, there is a lack of high-energy ps burst-mode lasers, and commercially available systems have repetition rates below 50 Hz.

To overcome the low-repetition-rate limitations of commercial, high-energy 100 ps systems and the peak power limitations of high-energy, ns burst-mode laser systems, a high-bandwidth, high-energy burst-mode laser of ~100 ps pulse duration has been developed by our group and demonstrated with operation at repetition rates of 10 kHz–1 MHz. The laser architecture utilizes both diode- and flashlamp-pumped Nd:YAG amplifiers for amplification of a nearly transform-limited 100 ps oscillator. The compact design is similar to that of previous burst-mode lasers that used narrow-bandwidth ns oscillators but with nearly two-orders-of-magnitude reduction in pulse duration [15,16]. As such, this laser will have wide applicability in an array of nonlinear spectroscopic and imaging applications in high-speed turbulent and unsteady reacting and nonreacting flows.

As shown schematically in Fig. 1, the master-oscillator is a custom mode-locked ps source (time–bandwidth products, GE-100-VAN-EJL) at 79.64 MHz with nominal pulse width of 100 ps at 1064.4100 (±0.0002) nm (vacuum). The oscillator is coupled to a single-mode (SM) polarization-maintaining (PM) fiber with 25% coupling efficiency (0.25 nJ per pulse). The repetition rate is reduced from 79.64 MHz to 10–1000 kHz using a fiber-coupled acousto-optic modulator (AOM). The suppression of

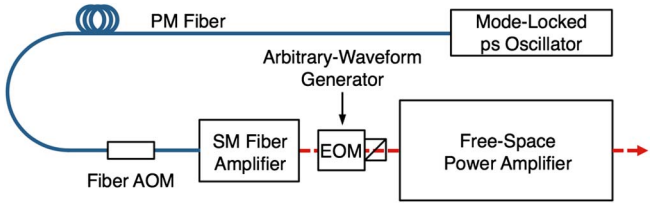

Fig. 1. Schematic of the mode-locked ps oscillator in conjunction with the burst-mode, free-space power amplifier. The acousto-optic modulator is used for pulse-rate reduction via a polarization-maintaining (PM) fiber before amplification in a single-mode (SM) fiber amplifier. A free-space electro-optic modulator (EOM) is used for burst shaping prior to the free-space power amplifier.

the pre- and post-pulse is greater than 10^3, ensuring a sequence of single pulses separated by 1–100 μs. The pulse sequence is amplified to 8.8 nJ/pulse in a single-mode fiber amplifier. While the output energy is limited to peak powers <100 W by stimulated-Brillouin scattering (SBS), the pre-amplification stage is a critical step in minimizing amplified spontaneous emission (ASE) in the initial free-space power amplifiers, particularly at low repetition rates (<50 kHz). To minimize further the ASE feedthrough from the fiber amplifier to the power amplifier, the pulse sequence is gated using a free-space electro-optic modulator (EOM) driven by an arbitrary-waveform generator. The EOM also can be used to increase burst uniformity by precompensating for the power-amplifier gain profile [16].

The free-space power amplifier (Fig. 1) consists of two single-pass and two double-pass diode-pumped amplifier modules with 2 and 5 mm diameter Nd:YAG rods, respectively, two single-pass flashlamp-pumped amplifier modules with 9.6 mm diameter Nd:YAG rods, and two single-pass flashlamp-pumped amplifier modules with 12.7 mm diameter Nd:YAG rods. The diode-pumped amplifiers are identical to those used for 100 ms burst generation, as described elsewhere [16]; however, the burst period in this work is restricted to 10 ms by the capacitance of the flashlamp-amplifier power supplies. The output of each amplifier is relay-imaged to the input of the succeeding amplifier to maintain high beam quality. Ceramic pinholes are located at the foci of the relay-imaging paths for spatial filtering and, therefore, minimize ASE between the amplifiers.

For reference, the free-space power amplifier was also operated with a ns-pulse-width oscillator, as described in previous work [16], with a full width at half-maximum (FWHM) of 7.9 ns, center wavelength of 1064.3847 (±0.0002) nm (vacuum), and spectral bandwidth of 480 MHz (HighFinesse, WS7 wavemeter). The ns oscillator was coupled to the fiber AOM and fiber amplifier via a PM fiber. To aid comparison, the ns-master-oscillator output was restricted to 9 nJ to match the ps-master-oscillator performance (8.8 nJ).

A direct comparison of ns and ps burst energy at 100 kHz (1000 pulses) is shown in Fig. 2(a) as a function of total flashlamp energy summed over all amplifiers. Under small-signal gain conditions (<1 kJ flashlamp energy), the ps burst energy is >94% of the corresponding ns burst energy. However, this value drops to ~85% as the power amplifier reaches saturation above 2 kJ flashlamp

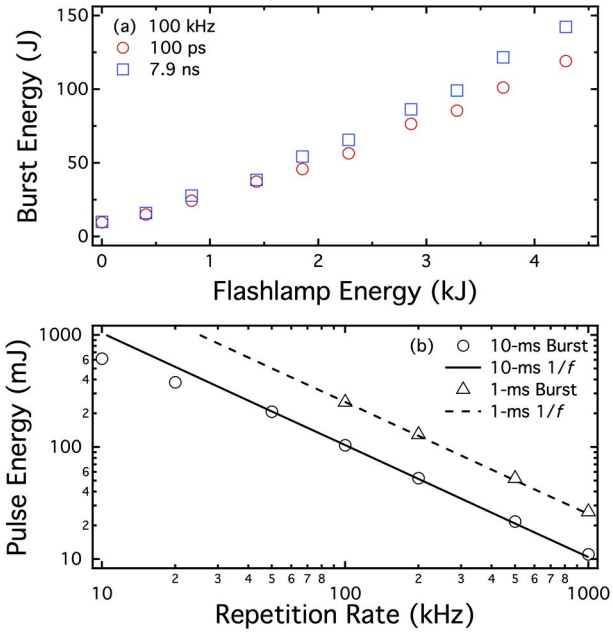

Fig. 2. (a) Total burst energy at 100 kHz as a function of total flashlamp energy for the 100 ps and 7.9 ns oscillators with a burst period of 10 ms. (b) Individual pulse energy at 1064 nm as a function of pulse repetition rate from 10–1000 kHz for a 10 ms burst (100–10,000 pulses) and for 1 ms burst operation from 100–1000 kHz (100–1000 pulses). Measurement uncertainty falls within the symbol size unless indicated.

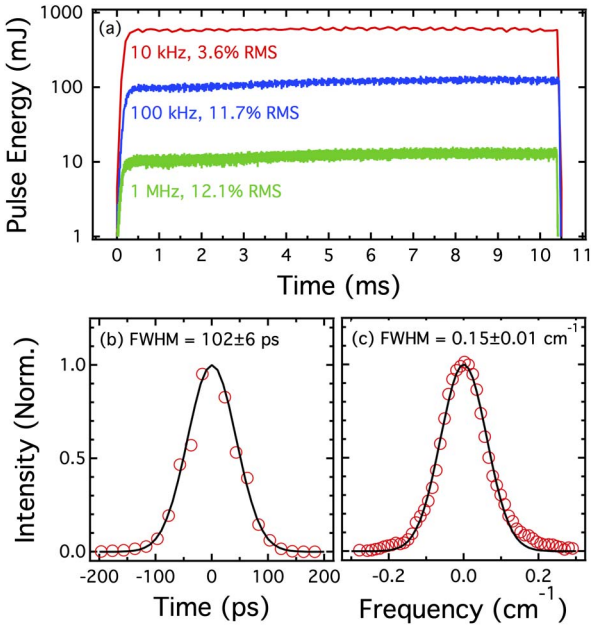

Fig. 3. (a) Burst profiles with 10.5 ms amplifier operation for repetition rates of 10 kHz, 100 kHz, and 1 MHz. (b) Pulse profile measured from autocorrelation with attained FWHM of 102 ± 6 ps. (c) Spectral bandwidth measured using an etalon with FWHM of 0.15 ± 0.01 cm^{-1}. The solid lines (b),(c) are Gaussian fits to experimental data (open symbols).

energy. This is attributed to the slight difference in center wavelength between the ns and ps oscillators, which results in reduced gain. Nevertheless, these data demonstrate efficient amplification of the ps pulse train in an Nd:YAG-based burst-mode laser.

Individual ps pulse energy is plotted as a function of pulse repetition rate, f, in Fig. 2(b). The power amplifier can be operated in a low-gain, 10 ms or high-gain, 1 ms configuration, constrained by the explosion limit of the individual flashlamps. For low-gain 600-V pumping over 10 ms, up to 615 mJ per pulse is available at 10 kHz (100 pulses), decreasing to 104 mJ at 100 kHz (1000 pulses) and 11 mJ at 1 MHz (10,000 pulses). In contrast, high-gain 800-V pumping over 1 ms yields a 2.4× increase in pulse energy, with 250 mJ per pulse at 100 kHz (100 pulses) and 26 mJ per pulse at 1 MHz (1000 pulses). The solid and dashed lines are $1/f$ scaling for the 10 and 1 ms bursts, respectively. At repetition rates <50 kHz, the measured pulse energy deviates from the $1/f$ scaling because of increased competition from ASE that results from longer inter-pulse periods. For comparison, the pulse energies at 50 kHz and a 10 ms burst period (207 mJ) and 100 kHz and a 1 ms burst period (250 mJ) are similar to the pulse energies available from commercial ps regenerative amplifiers that operate at 10 Hz and are used extensively for combustion diagnostics in reacting flows [6,8]. The system here is also nearly two orders of magnitude higher in energy than continuously pulsed, sub-ps Yb:YAG thin-disk amplifiers operating at similar repetition rates.

Burst profiles showing individual pulse energy over 10 ms are displayed in Fig. 3(a) for 10 kHz, 100 kHz, and 1 MHz pulse repetition rates. The time-averaged temporal profile and spectral bandwidth are shown in Figs. 3(b) and 3(c), respectively, for the laser pulse after second-harmonic generation to 532 nm. The pulse-to-pulse standard deviation across the burst increases from 3.6% at 10 kHz to 12.1% at 1 MHz. The variation is dominated by periodic oscillations in the efficiency of the AOM used to reduce the repetition rate from 79.64 MHz and is approximately two times higher than that reported for ns burst-mode lasers with similar energies [16]. The periodic oscillations in AOM efficiency originate from the independent phases of the AOM radio-frequency (RF) driving source and pulse train and, potentially, can be eliminated by phase locking the AOM RF driver and pulse train. The pulse-to-pulse variations are reduced at high energies because of saturation in the final stages of the power amplifier.

The temporal pulse width was measured via autocorrelation with a FWHM of 102 ± 6 ps assuming a purely Gaussian pulse profile. The spectral bandwidth was measured with a BK7-based etalon with nominal free spectral range of 10 GHz and finesse of 42. The measured bandwidth, FWHM of 0.15 ± 0.01 cm^{-1}, is within 5% of the transform limit.

For nonlinear spectroscopy, the primary advantage of ps laser pulses is high peak power associated with relatively narrow spectral bandwidth. This can be clearly observed by comparison of the second-harmonic generation (SHG) of the ps and ns burst-mode laser pulses. SHG conversion efficiency in a $15 \times 15 \times 18$-mm Type-II KD*P crystal ($\theta = 53.5°$) is plotted as a function of peak-power density in Fig. 4(a) for both ps and ns laser pulses. To permit direct comparison, the beam diameter was held constant at 6.5 mm in both cases. Maximum conversion efficiency of 16% is achieved for the ns

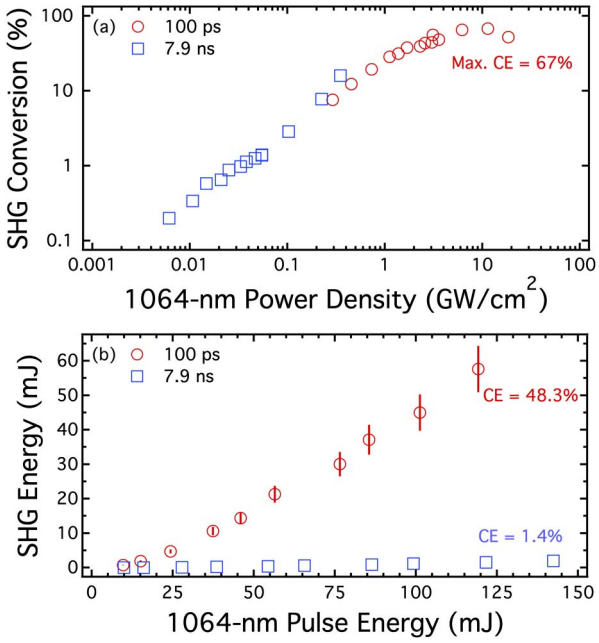

Fig. 4. (a) Second-harmonic conversion efficiency (SHG) in a $15 \times 15 \times 18$ mm Type-II KD*P crystal for 100 ps and 7.9 ns pulses as a function of 1064 nm power density. (b) Direct comparison of second-harmonic pulse energy at 100 kHz as a function of fundamental 1064 nm pulse energy for the 100 ps and 7.9 ns pulses under identical laser operating conditions.

SHG at 1064 nm pulse energy of 912 mJ. It should be noted that conversion efficiencies up to 55% have been demonstrated for ns burst-mode pulses with similar fundamental pulse energies using LBO crystal [21] but are limited here by crystal length and beam size, which were optimized for ps SHG. In contrast, 67% conversion efficiency is realized for 100 ps pulse widths and 1064 nm pulse energy of 380 mJ at 20 kHz. Above this limit the conversion efficiency decreases (52% at 10 kHz and 615 mJ) because of back conversion to 1064 nm, which occurs when the crystal length exceeds the optimal length for SHG. A maximum of 320 mJ per pulse is generated at 532 nm and 10 kHz.

The advantage of ps peak power is clearly evident from the direct comparison of SHG pulse energy for the ps and the ns sources in Fig. 4(b). At 100 kHz the maximum ns pulse energy is 2 mJ, while the ps pulse energy is 58 mJ, which represents a 30-fold increase under identical laser operating conditions. The ps conversion efficiencies match those achieved with traditional 10 Hz regenerative amplifiers.

In summary, the demonstrated ~100 ps, nearly transform-limited (~0.15 cm^{-1}), high-energy (up to 650 mJ/pulse), high-repetition-rate (10 kHz–1 MHz) burst-mode laser has sufficient performance characteristics for applicability in an array of linear and nonlinear spectroscopic and imaging applications in turbulent and unsteady reacting and nonreacting flows. In particular, the laser achieves a pulse width that has been shown in previous work to be ideal for performing (1) fiber-coupled CARS spectroscopy in gas-phase reacting flows, (2) interference-free, two-photon PLIF of atomic species, (3) real-time measurements of the collisional lifetime of molecular species such as CO or NO, and (4) Raman-excited laser-induced electronic fluorescence. Additionally, both the ns and ps oscillators could be simultaneously coupled to the power amplifier for pulse-width flexibility in a single system. Future work will include the application of these diagnostics for spatiotemporally resolved measurements in high-speed flows.

This work was funded by the Air Force Research Laboratory (FA8650-12-C-2200) and the Air Force Office of Scientific Research (Dr. Chiping Li, Program Manager).

References

1. D. Estruch, N. J. Lawson, and K. P. Garry, J. Aerospace. Eng. **22**, 383 (2009).
2. P. Wu and R. B. Miles, Opt. Lett. **25**, 1639 (2000).
3. B. Thurow, N. Jiang, and W. R. Lempert, Meas. Sci. Technol. **24**, 012002 (2013).
4. S. Roy, J. R. Gord, and A. K. Patnaik, Prog. Energy Combust. Sci. **36**, 280 (2010).
5. P. S. Hsu, W. D. Kulatilaka, J. R. Gord, and S. Roy, J. Raman Spectrosc. **44**, 1330 (2013).
6. T. B. Settersten, B. D. Patterson, and J. A. Gray, J. Chem. Phys. **124**, 234308 (2006).
7. R. B. Miles, J. J. Connors, E. C. Markovitz, P. J. Howard, and G. J. Roth, Exp. Fluids **8**, 17 (1989).
8. A. Bohlin and C. J. Kliewer, J. Chem. Phys. **138**, 221101 (2013).
9. W. D. Kulatilaka, H. U. Stauffer, J. R. Gord, and S. Roy, Opt. Lett. **36**, 4182 (2011).
10. H. Kalaycıoğlu, Y. B. Eldeniz, Ö. Akçaalan, S. Yavaş, K. Gürel, M. Efe, and F. Ö. Ilday, Opt. Lett. **37**, 2586 (2012).
11. S. Breitkopf, A. Klenke, T. Gottschall, H.-J. Otto, C. Jauregui, J. Limpert, and A. Tünnermann, Opt. Lett. **37**, 5169 (2012).
12. M. Schulz, R. Riedel, A. Willner, S. Düsterer, M. J. Prandolini, J. Feldhaus, B. Faatz, J. Rossbach, M. Drescher, and F. Tavella, Opt. Express **20**, 5038 (2012).
13. J. Körner, J. Hein, H. Liebetrau, R. Seifert, D. Klöpfel, M. Kahle, M. Loeser, M. Siebold, U. Schramm, and M. C. Kaluza, Opt. Express **21**, 29006 (2013).
14. I. Will, H. I. Templin, S. Schreiber, and W. Sandner, Opt. Express **19**, 23770 (2011).
15. M. N. Slipchenko, J. D. Miller, S. Roy, J. R. Gord, S. A. Danczyk, and T. R. Meyer, Opt. Lett. **37**, 1346 (2012).
16. M. N. Slipchenko, J. D. Miller, T. R. Meyer, J. Mance, S. Roy, and J. R. Gord, Opt. Lett. **39**, 4735 (2014).
17. M. J. Papageorge, T. A. McManus, F. Fuest, and J. A. Sutton, Appl. Phys. B **115**, 197 (2014).
18. J. D. Miller, M. N. Slipchenko, T. R. Meyer, N. Jiang, W. R. Lempert, and J. R. Gord, Opt. Lett. **34**, 1309 (2009).
19. N. Jiang, M. Webster, W. R. Lempert, J. D. Miller, T. R. Meyer, C. B. Ivey, and P. M. Danehy, Appl. Opt. **50**, A20 (2011).
20. J. B. Michael, P. Venkateswaran, J. D. Miller, M. N. Slipchenko, J. R. Gord, S. Roy, and T. R. Meyer, Opt. Lett. **39**, 739 (2014).
21. J. D. Miller, J. B. Michael, M. N. Slipchenko, S. Roy, T. R. Meyer, and J. R. Gord, Appl. Phys. B **113**, 93 (2013).
22. M. J. Papageorge, C. Arndt, F. Fuest, W. Meier, and J. A. Sutton, Exp. Fluids **55**, 1763 (2014).